Title

Microsecond simulation analysis of Carbonic anhydrase – II in complex with (+)-cathechin revealed molecular interactions responsible for its amelioration effect on fluoride toxicity

Authors

Pulala Raghuveer Yadav[1], Syed Hussain Basha[2], Sadam DV Satyanarayana[3], Pavan Kumar Pindi[3]

Affiliation

[1]: Department of Biotechnology, Indian Institute of Technology Hyderabad, Kandi, Sangareddy 502285, Telangana, India.
[2]: Innovative Informatica Technologies, Hyderabad 500049, Telangana, India.
[3]: Department of Microbiology, Palamuru University, Mahabubnagar 509001, Telangana, India.

Correspondence to be addressed

Email: pr.yadav@bt.iith.ac.in

or

pavankumarpindi@gmail.com

Abstract: Fluorosis is a chronic condition caused by overexposure to fluoride, marked by impaired dental, skeletal, and non-skeletal health. In presence of excess fluoride ions, in severe cases calcification of the ligaments observed. Earlier studies have suggested that the disruption of carbonic anhydrase activity via ionic homeostasis change was associated with F toxicity. In a recent study, it was demonstrated that Tamarind fruit extract was effective in increasing the urinary F excretion in male Wistar rats via studying the mRNA expression of carbonic anhydrase II (CA II) in kidney homogenates using western blotting, immunohistochemistry and quantitative Realtime PCR based studies. We have carried out this study to understand the detailed molecular level interactions responsible for this tamarind extract based (+)-cathechin compound towards lowering the F toxicity via targeting CA-II. From our study, it was revealed that due to the ability of (+)-cathechin compound to bind tightly filling complete available space at the catalytically important site forming metal coordinated ionic bonds with His94, His96 and His119 residues helps in restricting F ions to interact with Zn ion located at the core of catalytic site responsible for its functionality. On the other hand, interaction of (+)-cathechin compound with Gln92 was observed to be critically important towards inducing conformational changes in CA-II, thus allowing (+)-cathechin compound to burry even deeply inside the catalytic site.

Keywords: Fluorosis, carbonic anhydrase II, (+)-cathechin, tamarind fruit extract, molecular modeling, docking, MD simulations.

Introduction:

Globally, fluorosis is one of the ignored and sometimes disabling disease caused by excess fluoride consumption [1-2]. India, China, USA, Canada and Brazil are few of the majorly effected countries (figure 1) [3].

Figure 1: Shows fluorosis (dental and skeletal) worldwide.

Humans consume fluoride primarily from potable water in the regions where the water sources are affected with high fluoride concentration. As per the WHO guideline, the permissible limit of fluoride concentration in potable water is 1.5 mg/l [4] and as per the Bureau of Indian Standards, the desirable amount of fluoride concentration in potable water is 1.0 mg/L [5]. Additional sources of fluoride are foods rich in fluoride, air pollution from burning fluoride-rich coal and fluoride supplements. Fluoride in potable water exceeds 1.5 mg/L in the following countries United States of America, Germany, Norway, Kenya, Mexico, Niger, Nigeria, India, Indonesia,

Pakistan, Saudi Arabia, Israel, South Africa, Sudan, Spain, Japan, Sri Lanka, Senegal, Thailand, Turkey, Uganda, United Republic of Tanzania resulting in endemic fluorosis [6-7].

Millions of people woe from fluorosis throughout the world and the skeletal fluorosis effects acutely on the bones, making them crippled and leaving them to their beds. Thus it is sometimes a debilitating disease. As per the Government of India, as on April 2014, 230 districts in 19 Indian states were fluoride predominant with 14,133 habitations affected with fluoride over the permissible limits in 19 States/UTs with about 117.7 lakhs population at risk as shown below in the table 1 [8].

Table 1: State/Union Territory-Wise Details of Fluoride Affected Habitations & Population as on 01/04/2014:

S. No.	State/ Union Territory	Habitationss	Population
1.	Andhra Pradesh	745	1091394
2.	Bihar	893	491923
3.	Chhattisgarh	132	34720
4.	Goa	0	0
5.	Gujarat	63	90704
6.	Haryana	15	53455
7.	Himachal Pradesh	0	0
8.	Jammu & Kashmir	2	7911
9.	Jharkhand	12	5260
10.	Karnataka	1122	1329602
11.	Kerala	102	275557
12.	Madhya Pradesh	1055	454054
13.	Maharashtra	307	672939
14.	Odisha	279	55269
15.	Punjab	1	568
16.	Rajasthan	7670	4004613
17.	Tamil Nadu	0	0
18.	Telangana	1174	1922783
19.	Uttar Pradesh	180	143967
20.	Uttarakhand	2	10889
21.	West Bengal	251	178205
22.	Arunachal Pradesh	0	0
23.	Assam	128	58780
24.	Manipur	0	0
25.	Meghalaya	0	0

26.	Mizoram	0	0
27.	Nagaland	0	0
28.	Sikkim	0	0
29.	Tripura	0	0
30.	Andaman and Nicobar	0	0
31.	Chandigarh	0	0
32.	Dadra and Nagar Haveli	0	0
33.	Daman and Diu	0	0
34.	Lakshadweep	0	0
35.	Puducherry	0	0
	Total	**14133**	**11770593**

Source: https://pib.gov.in/newsite/PrintRelease.aspx?relid=107823

The supply of safe potable water, nutritional supplements and health services might avoid fluorosis in the future. Nevertheless, many people are already fluorosis affected and suffering for a long time and struggling to live.

Carbonic anhydrase – II (CA-II) (figure 2) is a metallo (zinc-containing) enzyme and is ubiquitous in nature; plays an important role in maintaining pH of the blood, bone resorption, acid base balance, urea genesis, production of body fluids and gluconeogenesis [9-10]. CA-II is found in animals and plants and even in the microbes. CA has different forms, structures, activities and belongs to α, β, γ, δ, and ζ families. It is essential to basic biological processes like CO2 and ion transport, acid-base balance calcification, respiration and photosynthesis [11-12]. The metal ion, Zn(II) acts as a cofactor, makes coordinate bonds with His94, His96, and His119 residues and a water molecule/hydroxide ion at the bottom of active-site cleft.

Exposure to high levels of F over a long period causes damage to osseous tissue, which results in skeletal and dental fluorosis [13]. Earlier studies have suggested that the disruption of carbonic anhydrase activity via ionic homeostasis change was associated with F toxicity [14-15].

In a recent study, it was demonstrated that Tamarind fruit extract was effective in increasing the urinary F excretion in male Wistar National Institute of Nutrition (NIN) rats via studying mRNA expression of carbonic anhydrase II (CA II) in kidney homogenates using western blotting, immunohistochemistry and quantitative Realtime PCR based studies [16-20].

In an another study by the same group, they have conducted molecular modeling and docking based studies on 12 phenolic compounds including (+)-cathechin, procyanidin, (–)-epicathechin, procyanidintrimer, procyanidin tetramer, procyanidinpentamer, procyanidinhexamer, taxifolin, apigenin, eriodictyol, luteolin, and naringenin from tamarind and reported that (+)-cathechin compound has best binding capability with CA-II [21]. Taking the queues from previous studies, we have carried out this study to understand the detailed molecular level interactions responsible for this tamarind extract based (+)-cathechin compounds amelioration effect on fluoride toxicity via targeting CA-II.

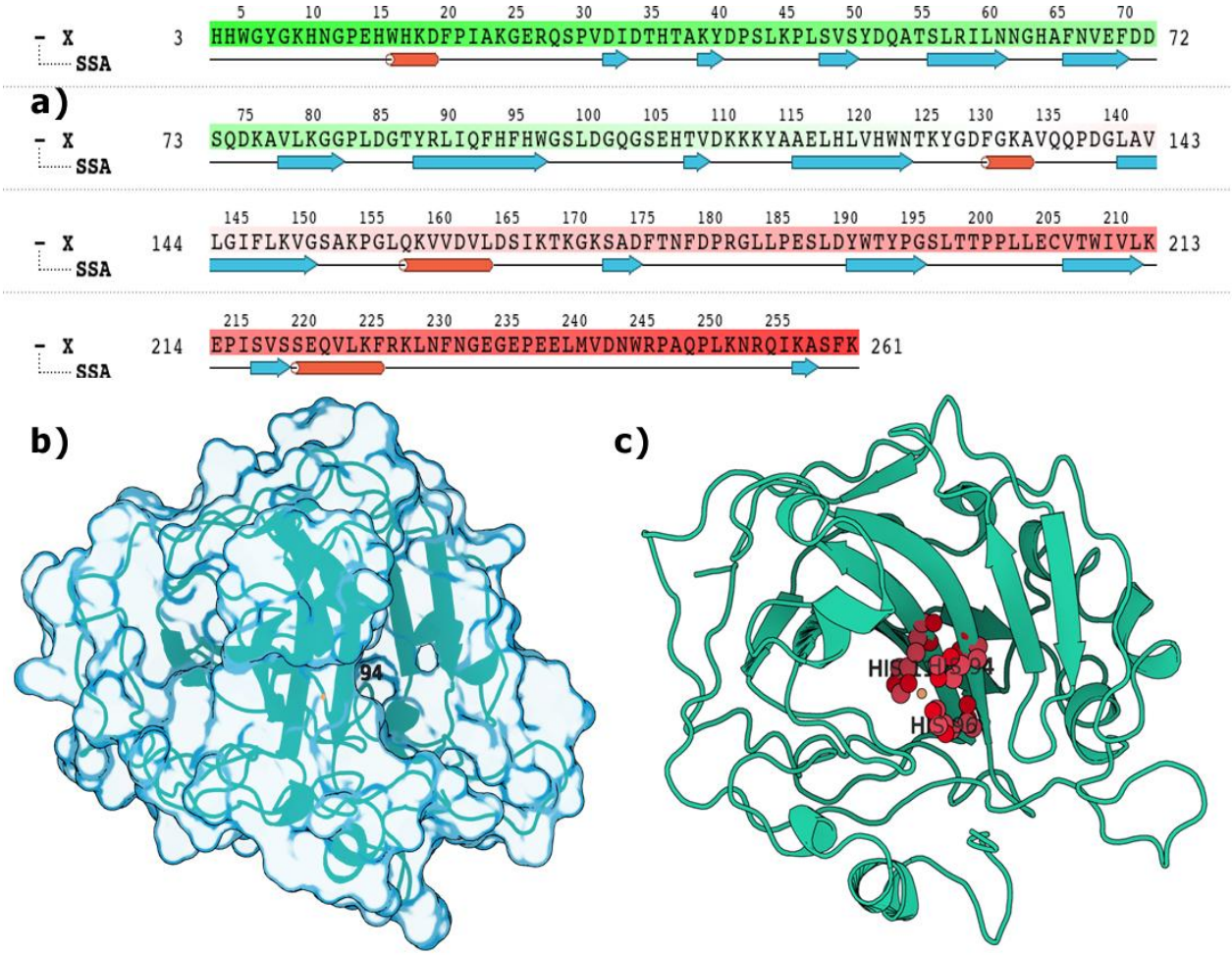

Figure 2: a) Amino acid sequence of Carbonic anhydrase – II (CA-II) **b)** 3D structure of CA-II in surface enabled mode and **c)** in ribbon model. Zinc ion surrounded by catalytic triad comprised of residues His94, His96 and His119 can be seen in the red color spheres.

Methods:

Schrodinger's maestro visualization program v9.6 [22] and Biovia Discovery studio v16.1 [23] were utilized to visualize the receptors, ligand structures, hydrogen bonding network, to calculate length of the bonds and to render images. Protein Imager [24] was used to visualize CA-II protein. (+)-cathechin compound (CID 9064) was retrieved from PubChem database [25]. Crystal structure of Carbonic anhydrase – II (CA-II) [PDB: 2VVB] was imported from the Protein Data Bank (PDB) [26]. Autodock 4.0 [27] is the preliminary docking program used

for the semi-flexible CA-II and (+)-cathechin compound docking studies. Preparation of the ligands and protein receptors in pdbqt file; determination of the size of the grid box size was done using Auto-Dock Tools version 1.5.6 using the default protocol as described elsewhere in detail [28-31]. Briefly, atomic salvation parameters 126 Å (x, y, and z) grid box for scoring energy was set centered at X = -9.688; Y = -1.652 and Z = 16.045 with 0.375 angstroms grid points spacing. Schrodinger's Desmond module v3.6 [32-33] was used for molecular dynamic simulation studies. OPLS 2005 force field [34] parameters have been applied to simulation TIP3P water models [35]. Periodic boundary conditions were used to determine the specific size and shape of the water box buffered at 10 Å distances and box volume was calculated as ~300000cubic Ås (for CA-II in its apo state and CA-II complexed with (+)-cathechin at its catalytic site) and ~350000cubic Ås (for CA-II in presence of F ions and for CA-II with (+)-cathechin at approximately 10 Ås distance from CA-II) of simulation box volume respectively (supplementary figure). Before starting the analysis, we have made sure that all the simulations were carried out at same temperature, pressure and volume conditions throughout of the simulated timescale. As part of the simulation quality analysis, it was revealed that average total energy of the simulated system remains the same as -90000kcal/mol in all cases of simulations (supplementary figure).

Results & Discussion:

In order to understand the dynamics of the CA-II in its apo form and CA-II in presence of F ions, we have performed two different molecular dynamic simulation of 1 microsecond (1000 nanoseconds) each. In one simulation, we have simulated CA-II in its apo form containing Zn ion surrounded by the catalytically important residues tightly bound by catalytic triad residues

His94, His96 and His119 (figure 3). Calculated distance between Zn ion and His94, His96 and His119 was 2.10 Å, 2.05 Å and 2.13 Å respectively (table 2). While, in another simulation we have randomly placed 18 F-ions covering all sides with ~5 Ås distance from peripheral residues of CA-II in its Apo form containing Zn ion.

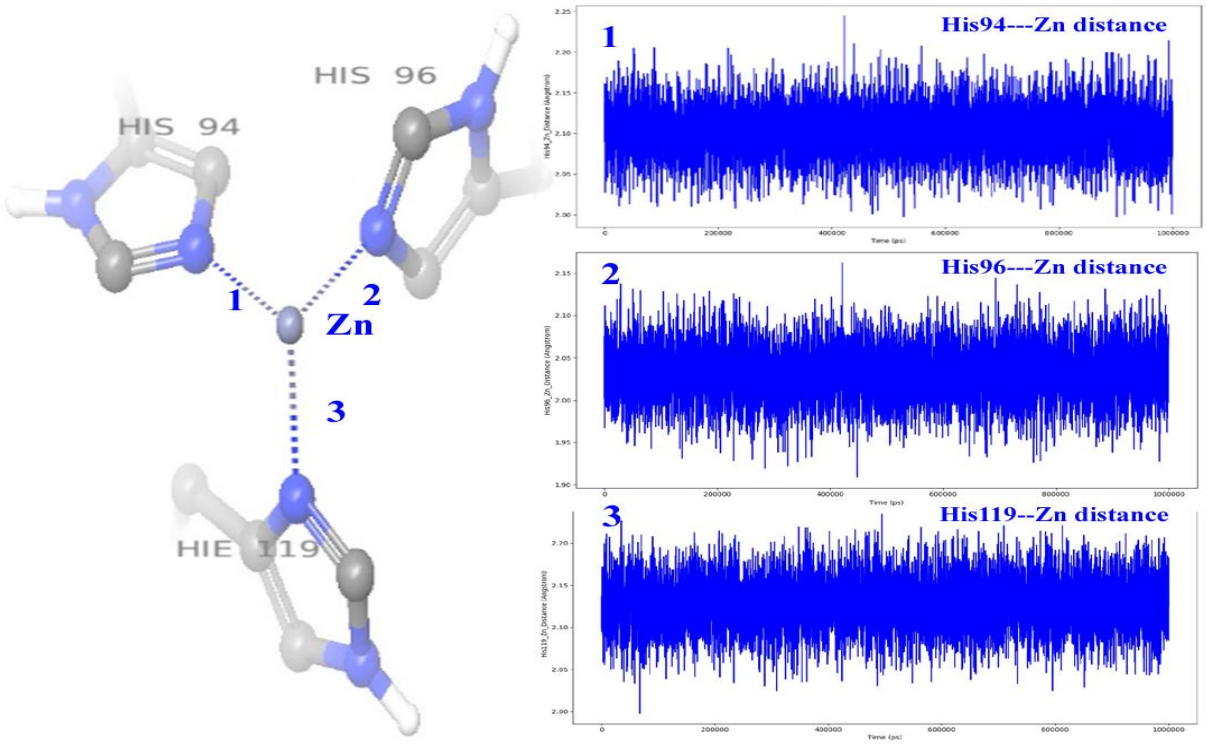

Figure 3: CA-II catalytic triad residues His94, His96 and His119 interactions with Zn ion (left). Right hand side three panels 1, 2 & 3 represents distance calculated between Zn ion and catalytic triad residues His94, His96 and His119. X-axis represents the simulation timescale in picoseconds (10000 picoseconds = 1000 nanoseconds i.e, 1 microsecond) and Y-axis represents the distance between the selected atoms in Å units.

Table 2: Calculated distance between Zn ion and catalytically important His94, His96 and His119 residues of CA-II in its apo form throughout the simulated timescale of 1 microsecond each.

S.No	Bond	Average bond length
1.	His94---Zn ion	2.10 Å
2.	His96---Zn ion	2.05 Å

3.	His119---Zn ion	2.13 Å

Analysis of CA-II dynamics during the simulated timescale:

In order to understand the CA-II dynamics, we have analyzed Root mean square deviation (RMSD) of protein backbone, Radius of Gyration (ROG) of protein, Root mean square fluctuations (RMSF) of individual residues in the protein, total number of intra molecular hydrogen bonds found within the protein (figure 4) and Secondary structural elements (SSE) percentage (figure 5) with reference to the simulated timescale. Protein's backbone RMSD was shown to be fluctuating between 1.5 and 3.0 Å, with an average of 2.2, 2.0, 2.5 and 2.4Å CA-II in its apo state, CA-II in presence of 18 F ions randomly placed in the simulated system, CA-II in presence of (+)-cathechin compound and 18 F ions randomly placed in the simulated system and CA-II in presence of (+)-cathechin compound complexed at the catalytic site simulations respectively. Calculated RMSD observed via superimposition of CA-II protein backbone at 500^{th} nanosecond from above mentioned simulations are tabulated in table 3. Notable conformational changes in the CA-II were observed between 300-500ns, especially in case of CA-II in presence of (+)-cathechin compound complexed at the catalytic site simulation. While, there was sudden jump in RMSD, ROG has shown to decrease at the same timescale of 300-500ns. However, no considerable changes were observed in total number of intra molecular hydrogen bonds observed during the entire simulated timescale. On the other hand, significant jump in the activity of individual residues RMSF upto 6Å was observed in case of CA-II in presence of (+)-cathechin compound complexed at the catalytic site simulation compared to other simulations data which remained below 3Å throughout simulated timescale on an average.

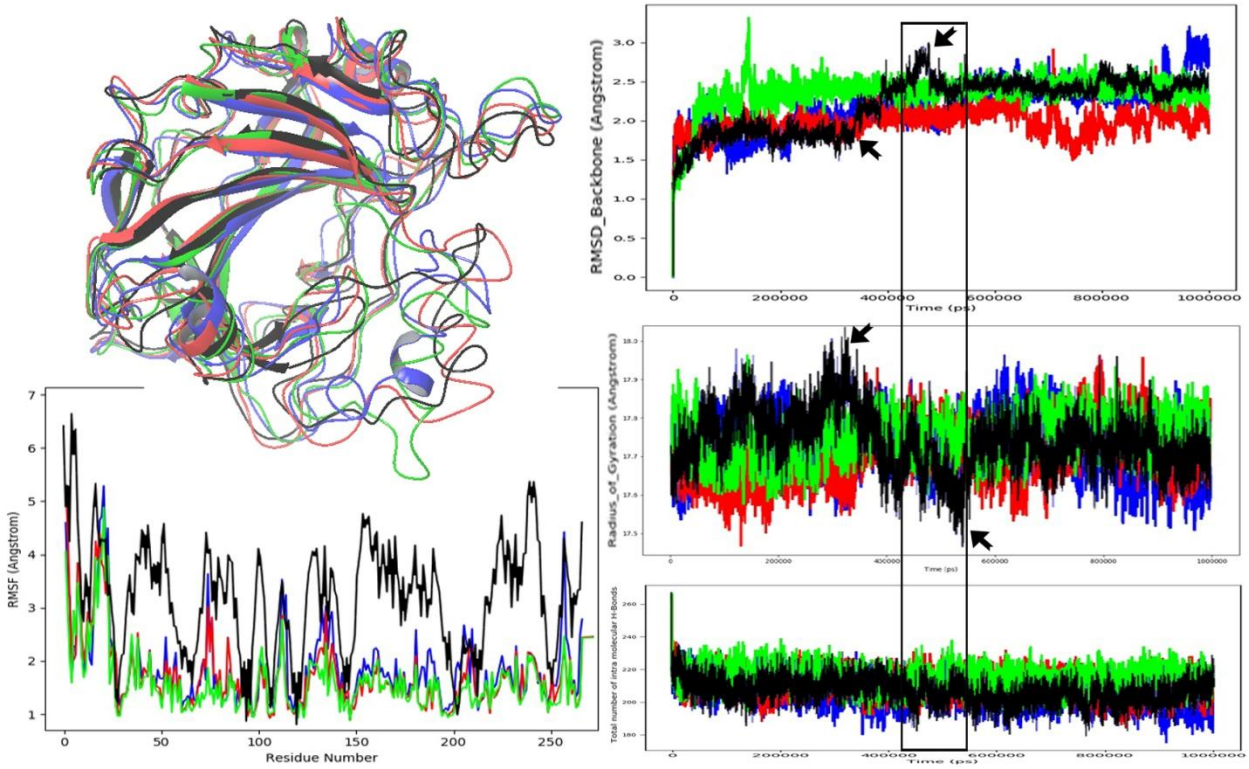

Figure 4: Dynamics of CA-II observed with reference to the simulated timescale. Blue, Green, Red and Black colors indicate CA-II in its apo state, CA-II in presence of 18 F ions randomly placed in the simulated system, CA-II in presence of (+)-cathechin compound and 18 F ions randomly placed in the simulated system and CA-II in presence of (+)-cathechin compound complexed at the catalytic site respectively. Left top figure shows the superimposition of the CA-II protein snapshot taken at 500th nanosecond from each simulation. 500th nanosecond was selected due to significant changes observed at that timeframe. Left bottom graph shows the RMSF of individual residues comparison among the simulations. Top right graph shows the RMSD of CA-II protein backbone comparison. Right middle graph shows the ROG of CA-II protein comparison and bottom right graph shows the total number of intra molecular hydrogen bonds observed within CA-II comparatively.

Table 3: Calculated Root mean square deviation (RMSD) of CA-II protein backbone superimposition:

S.No	Reference	Target	RMSD
1.	CA-II_apo (Blue)	CA-II_Catechin_dock (Black)	3.3965
2.	CA-II_F_ions (Red)	CA-II_Catechin_dock (Black)	2.8247
3.	CA-II_F_ions_catechin (Green)	CA-II_Catechin_dock (Black)	4.1752
4.	CA-II_Catechin_dock (Black)	CA-II_apo (Blue)	3.3960
5.	CA-II_F_ions (Red)	CA-II_apo (Blue)	2.8305
6.	CA-II_F_ions_catechin (Green)	CA-II_apo (Blue)	3.9778

From above RMSD, RMSF, ROG and intra molecular hydrogen bonds analysis, it was clear that some conformational changes in the protein are responsible for this inhibitory potential of (+)-cathechin compound. However, exactly which part of the protein is undergoing conformational changes towards this inhibitory along with potential abrogation of F ions interactions with ionic homeostasis remains in question. In order to find answer for this question, we have investigated the secondary structural elements (SSE) of the CA-II with reference to the simulated timescale. As can be seen from figure 5, few alpha-helices and beta-sheets at regions nearby to initial 20, 110, 160 and 180 residues have observed with significant changes. This loss of SSE was speculated to be responsible for higher RMSD, RMSF coupled with lowered ROG observed above, especially in the case of CA-II in presence of (+)-cathechin compound complexed at the catalytic site. Nevertheless, as observed in case of intra molecular hydrogen bonds, overall SSE percentage remained constant of about 35% throughout simulated timescale in all cases investigated (figure 6).

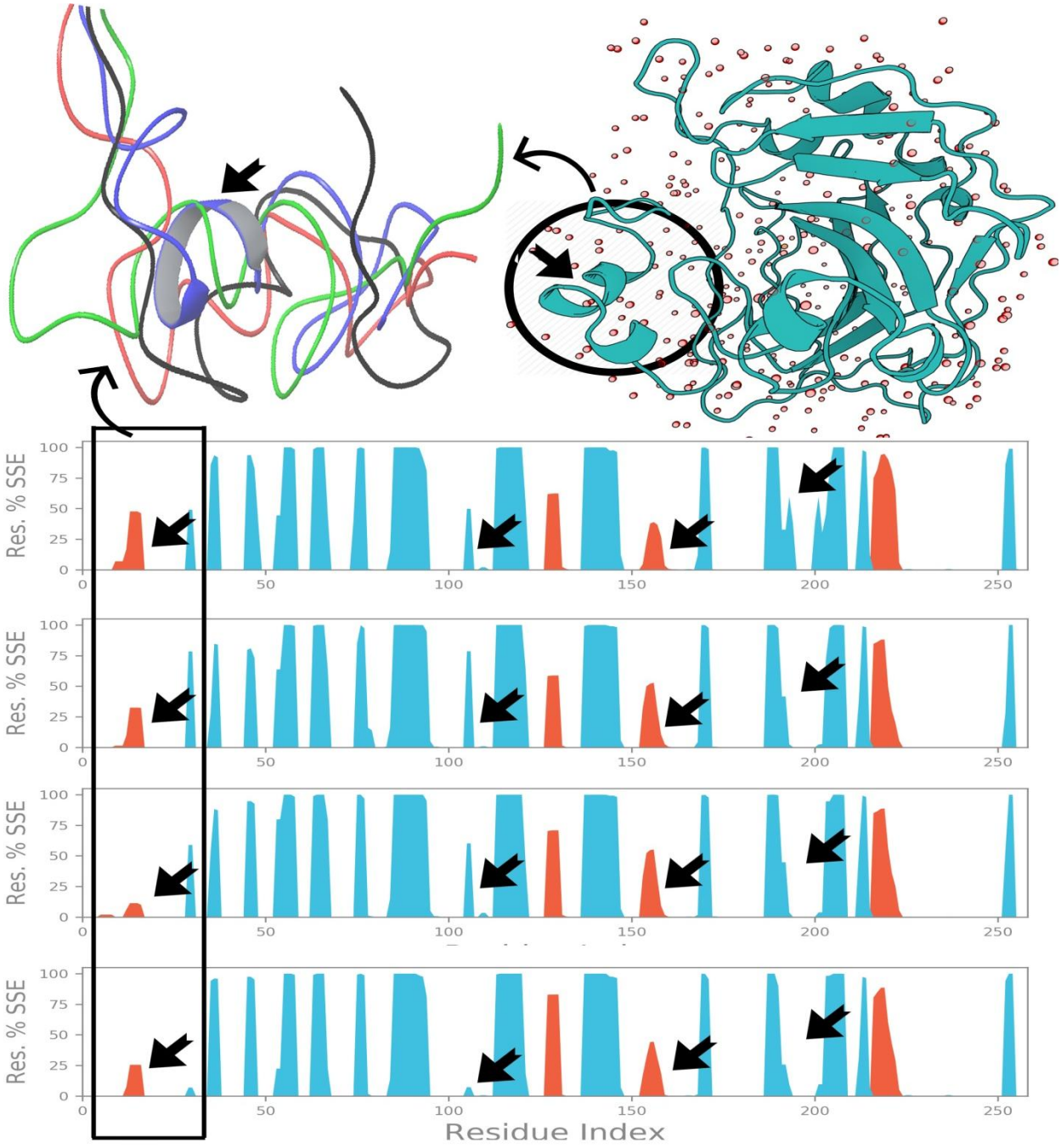

Figure 5: Secondary structural elements (SSE) percentage of Protein secondary structure elements (SSE) like alpha-helices (orange) and beta-strands (blue) are monitored throughout the simulation. In above plots X-axis represents residue index throughout the protein structure, while Y-axis represents SSE distribution for each trajectory frame over the course of the simulation. From top to bottom are the four charts representing CA-II in its apo state, CA-II in presence of 18 F ions randomly placed in the simulated system, CA-II in presence of (+)-cathechin compound and 18 F ions randomly placed in the simulated system and CA-II in presence of (+)-cathechin compound complexed at the catalytic site respectively. Top left figure shows the superimposition of CA-II from different studies simulations from present

investigation showing the alpha-helix region which was most affected during the simulation. Top right figure highlights the region of the CA-II which is used for the superimposition comparison.

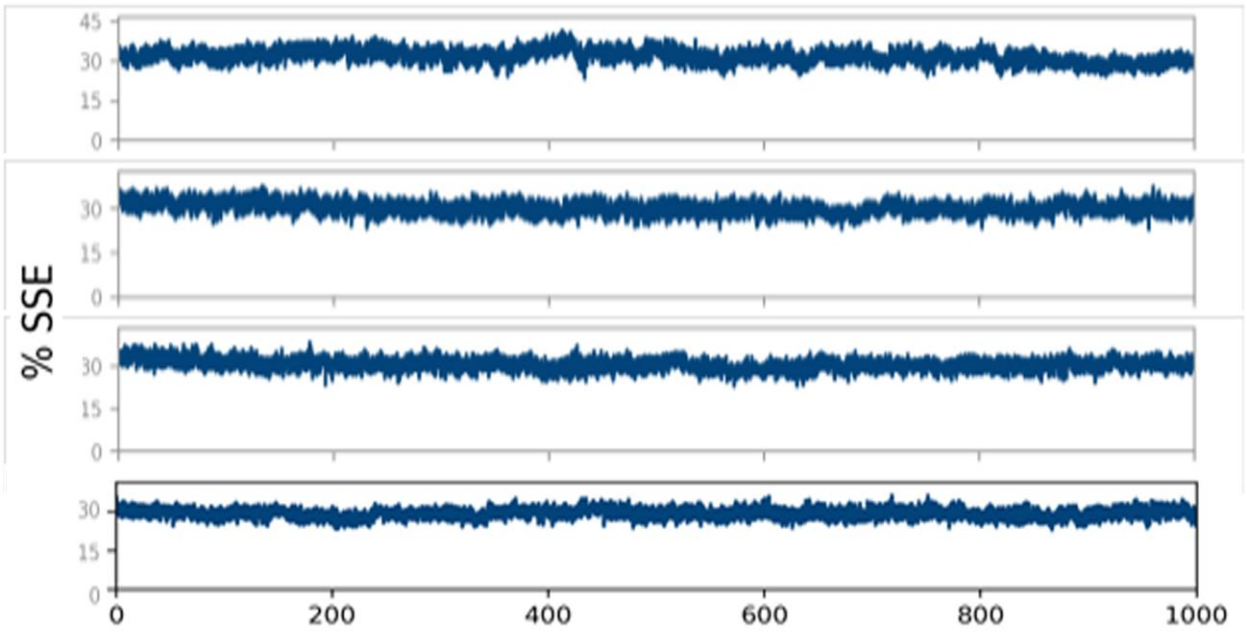

Figure 6: Comparison of percentage of Secondary structural elements (SSE) observed throughout the simulation. From top to bottom are SSE % representations of CA-II in its apo state, CA-II in presence of 18 F ions randomly placed in the simulated system, CA-II in presence of (+)-cathechin compound and 18 F ions randomly placed in the simulated system and CA-II in presence of (+)-cathechin compound complexed at the catalytic site respectively.

Molecular interactions between Carbonic Anhydrase – II (CA-II) with (+)-cathechin:

In order to understand the molecular level interactions between Carbonic Anhydrase – II (CA-II) and (+)-cathechin, we have performed two different molecular dynamics simulation of 1 micro second (1000 nanoseconds) each. In one simulation, we have randomly placed (+)-cathechin around 10 Å̊s distance from CA-II in order to provide unbiased freedom to the ligand to choose and bind at any place over CA-II and to study the protein behavior while this compound juggles around to find its binding place. While, in another simulation we have docked (+)-cathechin inside the binding pocket of CA-II targeting its catalytic traid comprised of His94, His96 and His119 residues, and then simulated the protein-ligand (CA-II + (+)-cathechin) complex towards

understanding impact of (+)-cathechin binding at CA-II catalytically important site. As per the docking results, it was found to be successfully binding at CA-II binding site, filling complete available space with a binding energy of -6.24 kcal/mol and predicted IC50 value of 26.51 uM (micromolar).

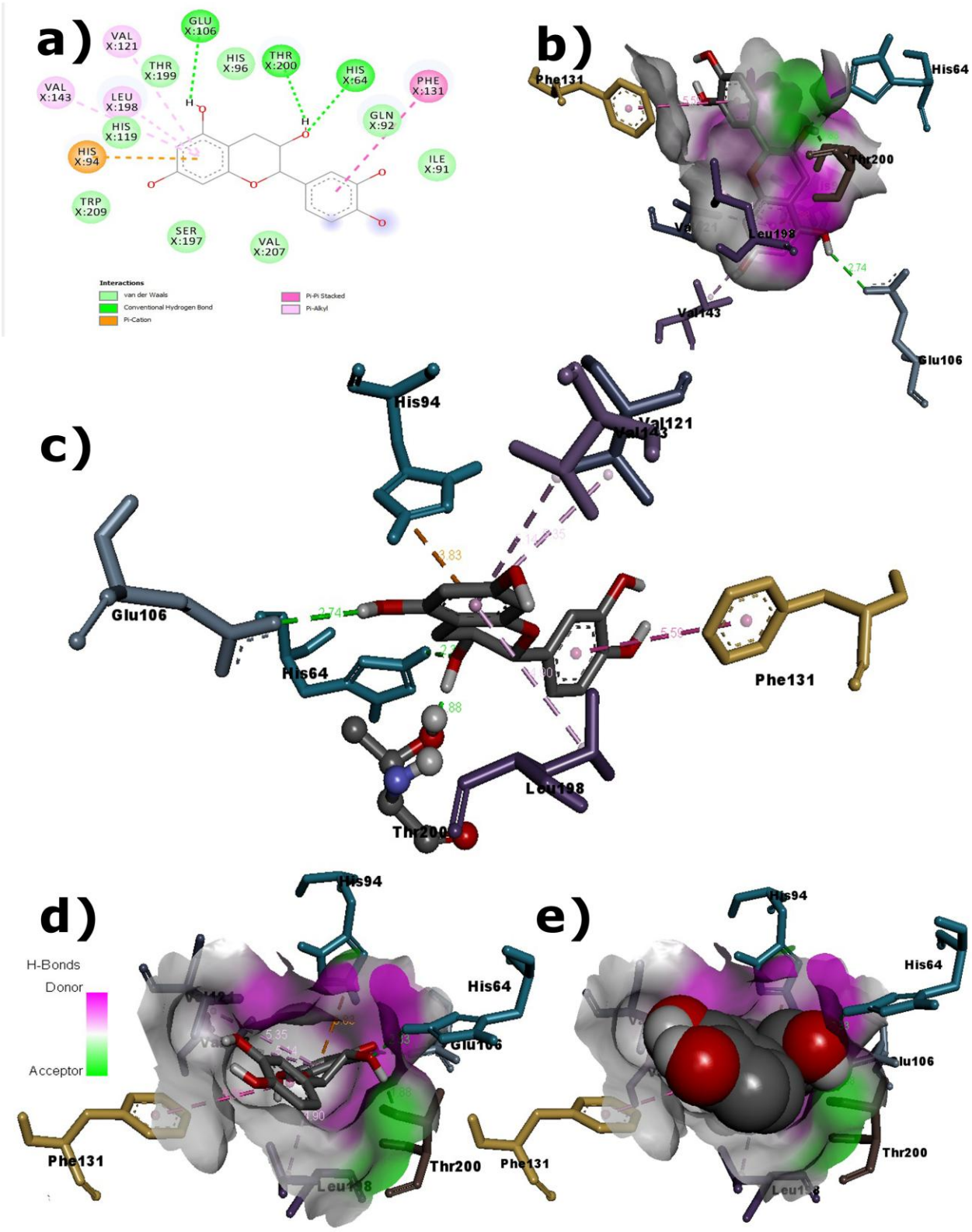

Figure 7: Molecular interactions observed between CA-II and (+)-cathechin compound based on docking: **a)** 2D interactions display **b)** side view of the compound binding inside the binding pocket **c)**

display of interactions in three dimensional space **d)** top view of the compound binding inside the binding pocket **e)** top view of the compound binding inside the binding pocket clearly depicting the complete binding pocket space filling as an indication of a tight binder. Amino acids are displayed in sticks model colored by amino acid. (+)-cathechin compound is displayed in stick model colored by elements.

As shown in figure 7, (+)-cathechin compound was found to successfully docked inside the active binding site forming direct hydrogen bonds with His64 (2.32 Å), Glu106 (2.74 Å) and Thr200 (1.88 Å). Residues Val143 (5.14 Å), Val121 (5.35 Å), Leu198 (4.90 Å) were observed to stacking with pi-alkyl interaction and Phe131 (5.59 Å) was observed to be forming a pi-pi stacking, while the catalytically important His94 (3.83Å) and His96 and His119 were found to be forming a pi-cation and van der waals interaction respectively (table 4).

Table 4: Calculated distance between (+)-cathechin compound and interacting residues including catalytically important His94, His96 and His119 residues of CA-II throughout the simulated timescale of 1 microsecond each.

S.No	Bond	Bond type	Average bond length
1.	His64---(+)-cathechin	Hydrogen bond	2.32 Å
2.	Glu106---(+)-cathechin	Hydrogen bond	2.74 Å
3.	Thr200---(+)-cathechin	Hydrogen bond	1.88 Å
4.	Val143---(+)-cathechin	pi-alkyl interaction	5.14 Å
5.	Val121---(+)-cathechin	pi-alkyl interaction	5.35 Å
6.	Leu198---(+)-cathechin	pi-alkyl interaction	4.90 Å
7.	Phe131---(+)-cathechin	pi-pi stacking	5.59 Å
8.	His94---(+)-cathechin	pi-cation interaction	3.83Å
9.	His96---(+)-cathechin	van der waals interaction	<5Å
10.	His119---(+)-cathechin	van der waals interaction	<5Å

To further investigate, we have taken the docked CA-II complexed with (+)-cathechin obtained from targeted docking for simulation. After successful completion of the simulation, we have analyzed the molecular level interactions between CA-II and (+)-cathechin responsible for its inhibitory effect. Throughout the simulation (+)-cathechin compound was observed to be maintaining 4-12 inter molecular hydrogen bonds with residues His3, His4, Trp5, Gly6, Tyr7, Asn11, Arg58, Asn61, Asn62, His64, Ala65, Phe66, Asn67, Val68, Glu69, Ile91, Gln92, His94, His96, Glu106, His119, Val121, Phe131, Val143, Lys170, Ser197, Leu198, Thr199, Thr200, Pro201, Trp209 and Asn244. Strikingly, catalytically important residues His94, His96 and His119 were in metal coordinated ionic bond formation including hydroxyl side chain of (+)-cathechin compound with Zn ion throughout the simulation timescale of 1000 nanoseconds. The same hydroxyl side chain of (+)-cathechin compound was also observed to be forming hydrogen bond with Glu106 residue for about 45% of the simulated timescale. His94 was observed to pi-stacked with (+)-cathechin compound for about 15% of the simulated timescale. (+)-cathechin was observed to so tightly bound at the catalytic site of CA-II that only part of the compound which showed some movement during the simulation was benzene ring composed of atoms 11-16 and associated hydroxyl groups composed of atoms 17 & 18 as revealed by the Root mean square fluctuations of individual atoms of the ligand (figure 8).

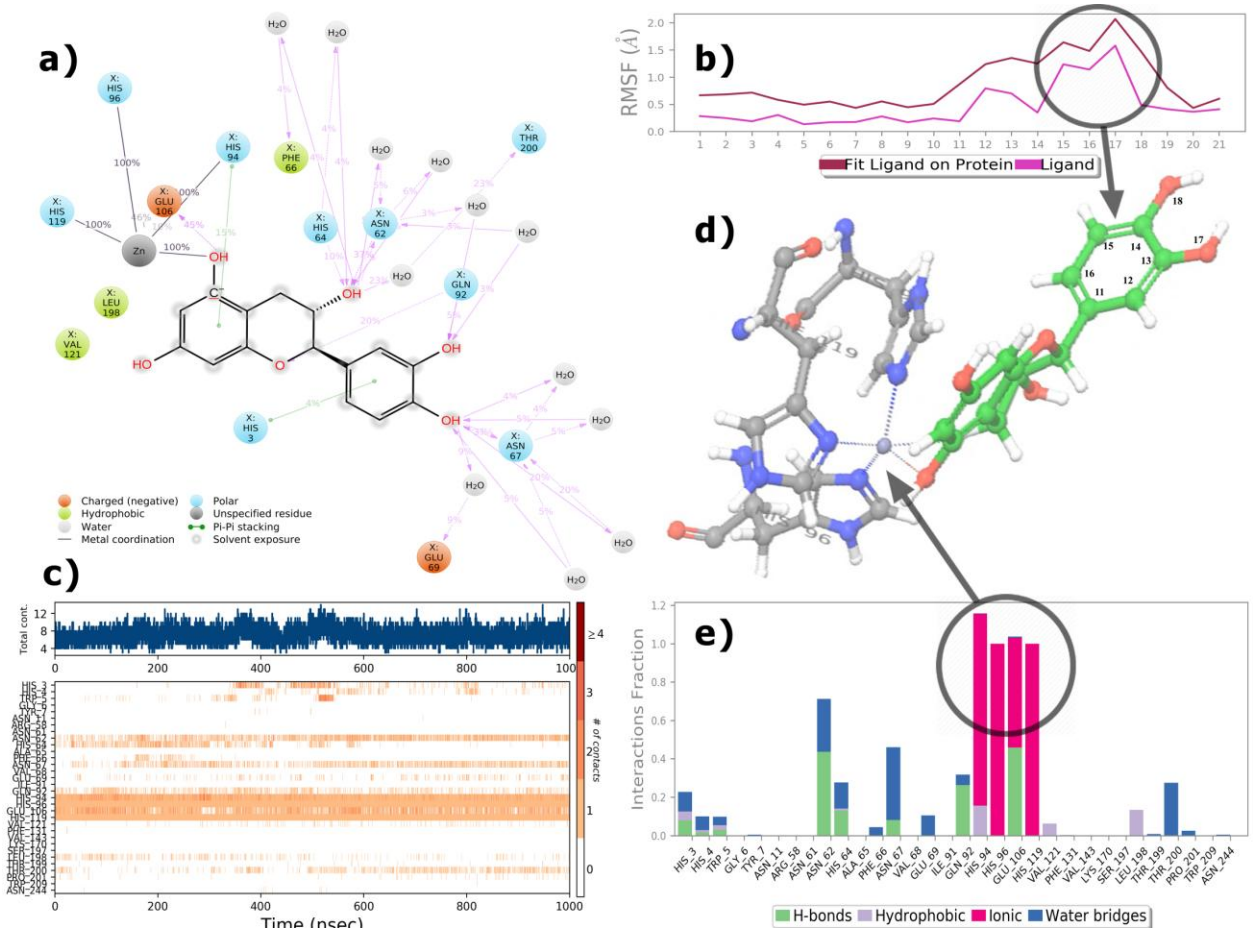

Figure 8: Molecular interactions observed between CA-II and (+)-cathechin compound at the catalytic site during simulated timescale of 1 microsecond. **a)** 2D interactions display between CA-II residues and **b)** RMSF of ligands individual atoms **c)** Heatmap of protein-ligand interactions showed by color intensity and total number of inter molecular interactions observed **d)** 3D visualization of (+)-cathechin compound interaction with Zn ion co-ordinated with ionic bonds with catalytic triad **e)** bar chart representing the percentage of timescale a specific interaction has been observed during the simulated timescale.

When other simulation, where (+)-cathechin compound was randomly placed approximately 10 Å distance from CA-II was analyzed it was revealed that the compound found juggling around the CA-II protein and never found and bind at the catalytically important site throughout 1 microsecond, but revealed many interesting interactions which might have lead to the conformational changes near the catalytic binding site to reveal itself attracting the binding of substrate. Among several residues, Asp72 was observed to be forming interactions with (+)-

cathechin for about 34% of the simulated timescale. While, other residues, Ile256, Leu47, Leu189, Glu205, Lys261, Arg89 and ASP190 were found to be interacting with (+)-cathechin for about 3-4% of the simulated timescale. Phe70, Asp71 and Ile91 were forming water molecules mediated interactions with (+)-cathechin for about 13% and 4% respectively for Phe70 and Asp71 & Ile91 (supplementary figures).

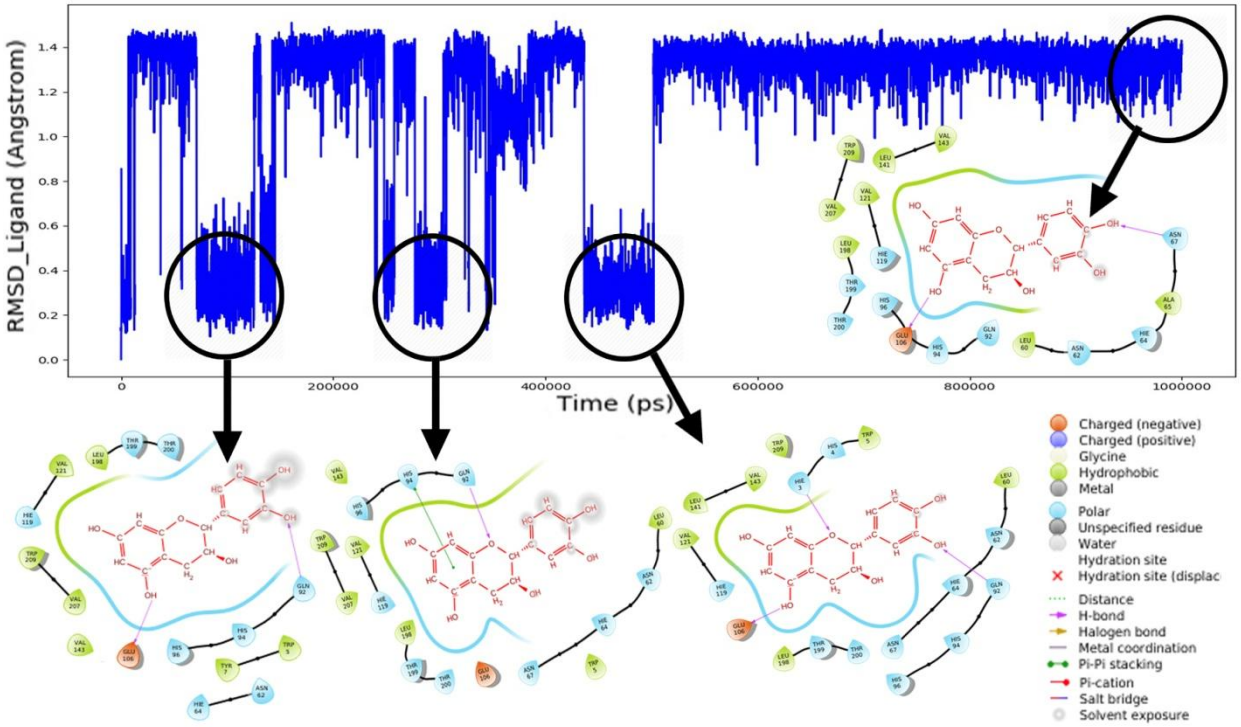

Figure 9: Ligand RMSD calculated throughout the simulated time scale of 1 microsecond. Circled are the timescale where snapshots have been sampled at 100ns, 300ns, 500ns and last frame respectively. A snapshot of (+)-cathechin at 100th nanosecond showed direct conventional hydrogen bonds with Gln92 and Glu106. (+)-cathechin at 300th nanosecond showed a pi-pi stacking with His94 along with a conventional hydrogen bond with Gln92. (+)-cathechin at 500th nanosecond showed three direct hydrogen bonds with His3, Gln92 and Glu106. Whereas the last snapshot of the simulation representing the majority of Ligand RMSD at 1.4Å revealed couple of direct hydrogen bonds with Asn67 and Glu106 residues.

Since (+)-cathechin bound at catalytic binding site simulation showed interesting interactions, we have taken the analysis further to understand the ligand Root mean square deviation (RMSD) throughout the simulated timescale and the interactions responsible at some key events (figure

9). On an average ligand RMSD was maintained upto 1.4Å which is quite stable in itself, however at some points of simulations the RMSD has sudden drop upto 0.2Å. These dramatic changes in the ligand RMSD caught our attention. To investigate these events further, we have sampled four snapshots during the simulation; three snapshots at 100ns, 300ns and 500ns each along with a snapshot at the end of the simulation. Among the interactions found responsible, Gln92 was found to be the only difference between snapshots which were observed at 0.2Å and 1.4Å. From this analysis, we can presume that the interaction of the substrate with Gln92 is triggering significant conformational changes in the CA-II towards lowering the ligand RMSD and thus stabilizing it via binding tightly.

Furthermore, from our analysis it was revealed that (+)-cathechin compound + CA-II complex follows the type I inhibition mechanism via coordination of the inhibitor to the Zn(II) ion by replacing the zinc-bound water/hydroxide ion and leading to a tetrahedral geometry of Zn(II) as per Derya Ekinici et.al. [36]

Conclusion:

In this present study, we have made an attempt to understand the molecular level interactions responsible for the (+)-cathechin amelioration effect on fluoride toxicity targeting Carbonic anhydrase – II (CA-II) using molecular modeling and simulations based computational approaches. From our study, it was revealed that due to the ability of (+)-cathechin compound to bind tightly filling complete available space at the catalytically important site forming metal coordinated ionic bonds with His94, His96 and His119 residues helps in restricting F ions to interact with Zn ion located at the core of catalytic site responsible for its functionality. On the other hand, interaction of (+)-cathechin compound with Gln92 was observed to be playing a

crucial role in causing conformation changes in CA-II and thus allowing (+)-cathechin compound to burry even deeply inside the catalytic site. On the other hand, conversion of alpha-helices and beta-sheets to loops at regions nearby to initial 20, 110, 160 and 180 residues were thought to be regulating substrate binding trajectory. Molecular interactions detailing and identification of potential regions in the CA-II responsible for its activity via microsecond level simulations obtained in this present study is thought to be helpful in conducting future studies towards optimizing ligands further for better amelioration effect on fluoride toxicity.

Authors' contribution: Pulala Raghuveer Yadav designed the study. Syed Hussain Basha and Pulala Raghuveer Yadav executed the work and generated the data. Pulala Raghuveer Yadav, Syed Hussain Basha, Sadam DV Satyanarayana and Pavan Kumar Pindi analyzed the data and wrote the manuscript. All authors have read and approved the final manuscript.

Conflicts of Interest: The authors declare that they have no conflict of interests.

References:

1. Environment Health Criteria 227: Fluorides; Liteplo, R.; Howe, P.; Malcolm, H., Eds.; International Programme on Chemical Safety, World Health Organization: Geneva, 2002; p 268.
2. Ullah, Rizwan, Muhammad Sohail Zafar, and Nazish Shahani. "Potential fluoride toxicity from oral medicaments: A review." *Iranian journal of basic medical sciences* 20.8 (2017): 841.
3. Adapted from WHO. Inheriting the World: The Atlas of Children's Health and the Environment; Gordon, B., Mackay, R., Rehfuess, E., Eds.; World Health Organization: Geneva, 2004.
4. WHO (2011) Guidelines for drinking-water quality, 4th edn, vol 1: recommendations. World Health Organization, Geneva.
5. Bureau of Indian Standards. Indian Standard drinking water-specification.2nd revision. New Delhi: Bureau of Indian Standards; 2012.p.2
6. A.K. Susheela (2002). Fluoride in developing countries: Remedial measures and approaches. *Proceedings of the Indian National Science Academy, B68 No.5*.
7. Jarvis, Helen G., et al. "Prevalence and aetiology of juvenile skeletal fluorosis in the south- west of the H ai district, T anzania–a community- based prevalence and case–control study." *Tropical Medicine & International Health* 18.2 (2013): 222-229.

8. Del Bello, Lou. "Fluorosis: an ongoing challenge for India." *The Lancet Planetary Health* 4.3 (2020): e94-e95.

9. Kivela A, Parkkila S, Saarnio J, Karttunen TJ, Kivela J, Parkkila AK, Waheed A, Sly WS, Grubb JH, Shah G, Tureci O, Rajaniemi H (2000) Expression of a novel transmembrane carbonic anhydrase isozyme XII in normal human gut and colorectal tumors. Am J Pathol 156:577–584).

10. Lehtonen J, Shen B, Vihinen M, Casini A, Scozzafava A, Supuran CT, Sly WS (2004) Characterization of CA XIII, a novel member of the carbonic anhydrase isozyme family. J Biol Chem 279:2719– 2727.

11. Smith, K. S., Ferry, J. G., Prokaryotic carbonic anhydrases. FEMS Microbiol. Rev. 2000, 24, 335–366.

12. Smith, K. S., Ferry, J. G., A plant-type (β-class) carbonic anhydrase in the thermophilic methanoarchaeon Methanobacterium thermoautotrophicum. J. Bacteriol. 1999, 181, 6247–6253.

13. Whitford GM (1996) The metabolism and toxicity of fluoride. Monogr Oral Sci 2:1–153.

14. Birchard GF, Black CP (1986) Effect of carbonic anhydrase inhibition on blood acid-base balance in the chicken embryo. Poult Sci 65:1811–1813.

15. Shashi A, Meenakshi G (2015) Evaluation of cytosolic erythrocyte carbonic anhydrase in fluorosis. J Basic Appl Res Int 3:108–115.

16. Khandare, Arjun L., et al. "Tamarind fruit extract ameliorates fluoride toxicity by upregulating carbonic anhydrase II: a mechanistic study." *Fluoride* 51.2 (2018): 137-152.

17. Khandare AL, Kumar PU, Lakshmaiah N. Beneficial effect of tamarind ingestion on fluoride toxicity in dogs. Fluoride 2000;33(1):33-8.

18. Khandare AL, Rao GS, Lakshmaiah N. Effect of tamarind ingestion on fluoride excretion in humans. Eur J Clin Nutr 2002;56(1):82-5.

19. Khandare AL, Kumar PU, Shanker RG, Venkaiah K, Lakshmaiah N. Additional beneficial effect of tamarind ingestion over defluoridated water supply to adolescent boys in a fluorotic area. Nutrition 2004;20(5):433-6.

20. Vasant RA, Narasimhacharya AV. Ameliorative effect of tamarind leaf on fluoride-induced metabolic alterations. Environmental health and preventive medicine. 2012 Nov;17(6):484.

21. Manne, Munikumar, Vakdevi Validandi, and Arjun L. Khandare. "Reduction of fluoride toxicity by tamarind components: an in silico study." *Fluoride* 51.2 (2018): 122-136.

22. Schrödinger Release 2013-2: Maestro, Schrödinger, LLC, New York, NY, 2013.

23. *Dassault Systèmes BIOVIA, Discovery studio, version 16.1, San Diego: Dassault Systèmes, 2019.*

24. Gianluca Tomasello, Ilaria Armenia, Gianluca Molla, The Protein Imager: a full-featured online molecular viewer interface with server-side HQ-rendering capabilities, Bioinformatics, Volume 36, Issue 9, 1 May 2020, Pages 2909–2911, https://doi.org/10.1093/bioinformatics/btaa009

25. Kim, Sunghwan, et al. "PubChem substance and compound databases." *Nucleic acids research* 44.D1 (2016): D1202-D1213.

26. Sussman, Joel L., et al. "Protein Data Bank (PDB): database of three-dimensional structural information of biological macromolecules." *Acta Crystallographica Section D: Biological Crystallography* 54.6 (1998): 1078-1084.

27. Forli, William E. Hart, et al. "AutoDock Version 4.2." (2012).

28. Reddy, S. V. G., et al. "Molecular docking and dynamic simulation studies evidenced plausible immunotherapeutic anticancer property by Withaferin A targeting indoleamine 2, 3-dioxygenase." *Journal of Biomolecular Structure and Dynamics* 33.12 (2015): 2695-2709.

29. Murthy, NVS Viswanadha. "M, V. Girija Sastry, Syed Hussain Basha.(2018) 3, 5-dinitrophenyl clubbed azoles against latent tuberculosis-a theoretical mechanistic study." *Journal of PeerScientist* 1.1: e1000001.

30. Rao, Chennu Maruthi Malya Prasada, et al. "Molecular docking based screening of novel designed chalcone series of compounds for their anti-cancer activity targeting EGFR kinase domain." *Bioinformation* 11.7 (2015): 322.

31. Rao, CH MM Prasada. "Novel series of 1, 5 Benzothiazepine skeleton based compounds as anti-cancer agents–In silico and MTT assay based study." *Journal of PeerScientist* 1.2 (2018): e1000008.

32. Kevin J. Bowers, Edmond Chow, Huafeng Xu, Ron O. Dror, Michael P. Eastwood, Brent A. Gregersen, John L. Klepeis, Istvan Kolossvary, Mark A. Moraes, Federico D. Sacerdoti, John K. Salmon, Yibing Shan, and David E. Shaw, "Scalable Algorithms for Molecular Dynamics Simulations on Commodity Clusters," *Proceedings of the ACM/IEEE Conference on Supercomputing (SC06), Tampa, Florida*, 2006, November 11-17.

33. Schrödinger Release 2020-2: Desmond Molecular Dynamics System, D. E. Shaw Research, New York, NY, 2020. Maestro-Desmond Interoperability Tools, Schrödinger, New York, NY, 2020.

34. McDonald, Nora A., and William L. Jorgensen. "Development of an all-atom force field for heterocycles. Properties of liquid pyrrole, furan, diazoles, and oxazoles." *The Journal of Physical Chemistry B* 102.41 (1998): 8049-8059.

35. Mark, Pekka, and Lennart Nilsson. "Structure and dynamics of the TIP3P, SPC, and SPC/E water models at 298 K." *The Journal of Physical Chemistry A* 105.43 (2001): 9954-9960.

36. Ekinci, Derya, et al. "Carbonic anhydrase inhibitors: in vitro inhibition of α isoforms (hCA I, hCA II, bCA III, hCA IV) by flavonoids." *Journal of enzyme inhibition and medicinal chemistry* 28.2 (2013): 283-288.